SUPPORTING INFORMATION

H-Aggregation Induced Dual Emissive Carbon Nanoparticles for Ratiometric Detection of Uranyl Ions through Dynamic to Static Excimer Formation

±Md. Abdus Salam Shaik[a][c], ±Dipanjan Samanta[a], ±Manisha Shaw[a], Ankit Kumar Sharma[a], Sayan Prodhan[b], Imran Mondal[a], Rajarshi Basu[a], Angana Bhattacharya[a], Shumaila Masood[d], Prasanta Kumar Datta[b], Amita Pathak[a]*

±*Contribute equally to this work*

[a]*Department of Chemistry, Indian Institute of Technology Kharagpur, West Bengal, India -721302*

[b] *Department of Physics, Indian Institute of Technology Kharagpur, West Bengal, India -721302*

[c] *Department of Mathematics and Basic Science, NIIT University, Rajasthan, India -301705*

[d] *Department of Food Science and Technology, United Arab Emirates University, Al Ain, UAE*

* Corresponding Author
Prof. Amita Pathak
Email id: ami@chem.iitkgp.ac.in

**Instrument used for the characterization of CNPs:**

Particle distribution and the morphology of synthesized CNPs were shown by transmission electron microscope (TEM) in a TECNAI G2 20S-TWIN (Japan) machine with an acceleration voltage of 200 kV. Alcoholic solution of CNPs was prepared for TEM measurement, where the sample was well distributed and drop casted into a 300-mesh carbon-coated copper cast and the solvent were evaporated for overnight at room temperature. XRD analysis of water soluble CNPs was carried out using an X-ray Diffractometer (Bruker, ModelD8 powder XRD) with Cu-Kαradiation over the 2θ range of 12 to 70˚. FT-IR spectrum was carried out within 4000–400 cm⁻¹ range in a Perkin-Elmer Spectrum RX-II (Model no. 73713, USA) instrument to confirm the presence of different functional groups of CNPs. The UV-Vis spectra and fluorescence emission spectra were taken by using a UV-vis spectrophotometer (SHIMADZU UV-2450, Japan) and fluorescence emission spectra were recorded in a Fluorescence spectrophotometer (HITACHI F-7000, Japan). Aggregation of the as CNPs was identified by using circular dichroism spectrometer on a JASCO-810 automatic recording spectrophotometer under a constant nitrogen flow at 25 °C. The CD spectra were acquired in a strain free quartz cuvette of 0.1 cm path length, in the wavelength range of 200 to 750 nm at a scan rate of 50 nm per min. Circularly polarized luminescence (CPL) experiments were carried out on a Jasco CPL-300 spectrophotometer having digital integration time (D.I.T) fixed at 4.0 seconds with multiple spectral accumulations. The X-ray photoelectron spectrum (XPS) of CNPs was recorded in a PHI 5000 Versa probe-II scanning microprobe (United States) outfitted with an Al-Kα X-ray monochromator (1486.7 eV). The binding energy scale of the spectrum has been calibrated by standard value of C 1s at 284.6 eV. 2.5.
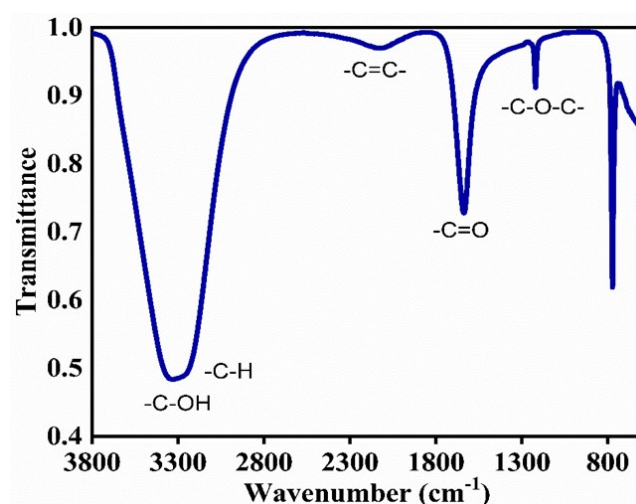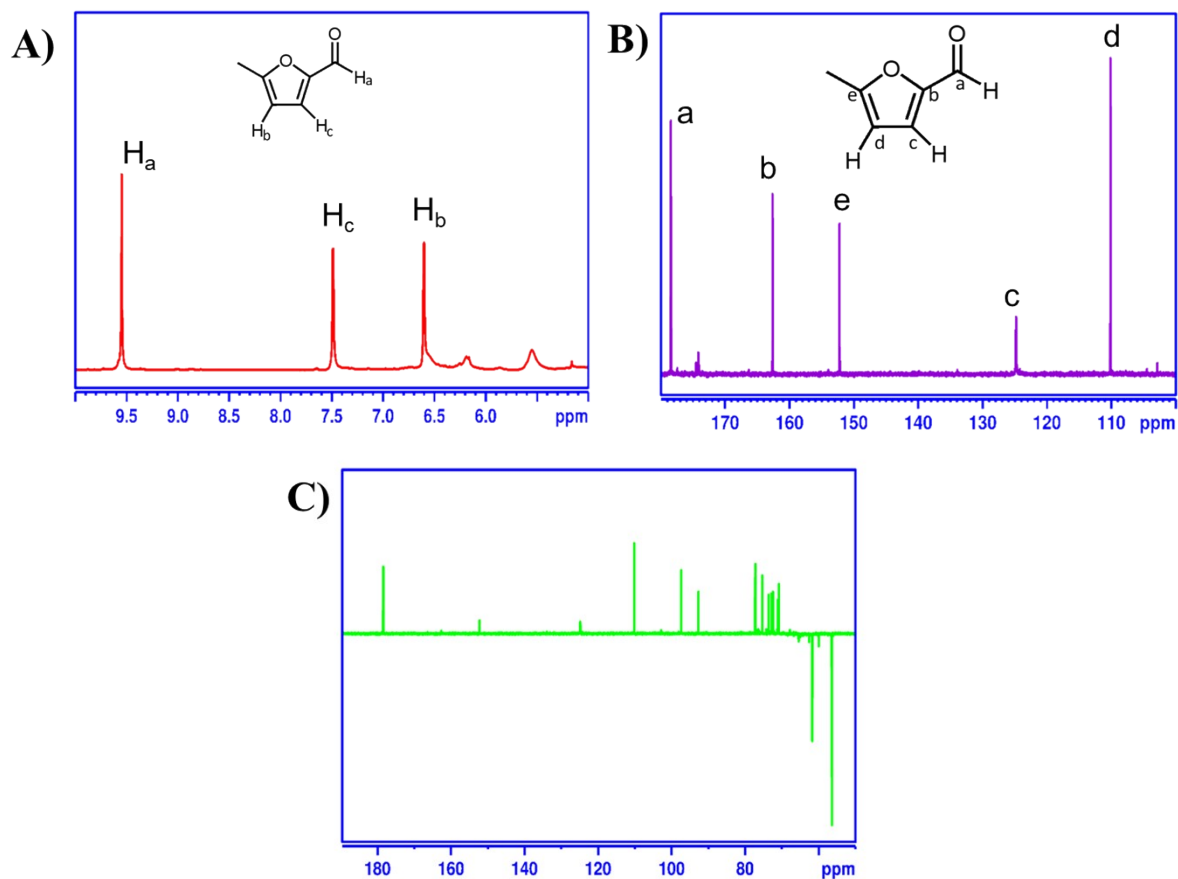

Fig S1: FTIR spectrum of CNPs
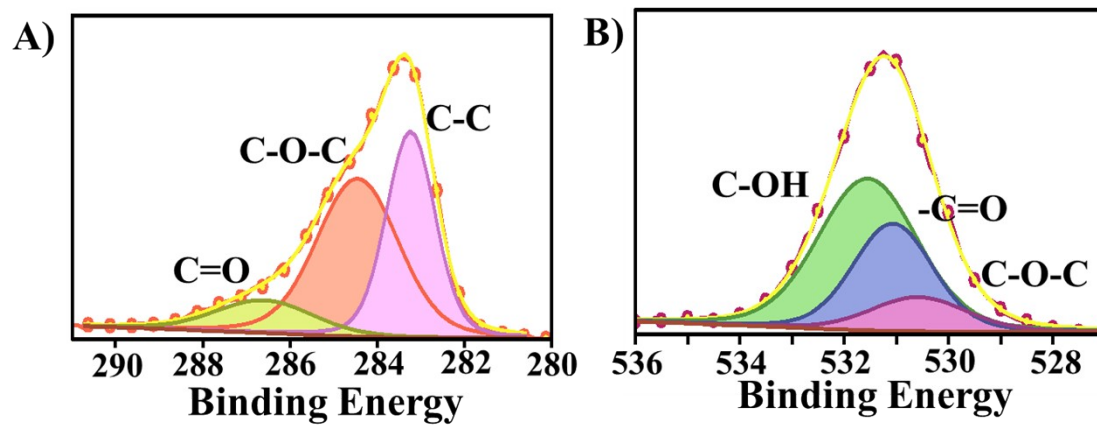
**Fig S2**: Deconvulated XPS spectra of A) C1s B) O1s CNPs
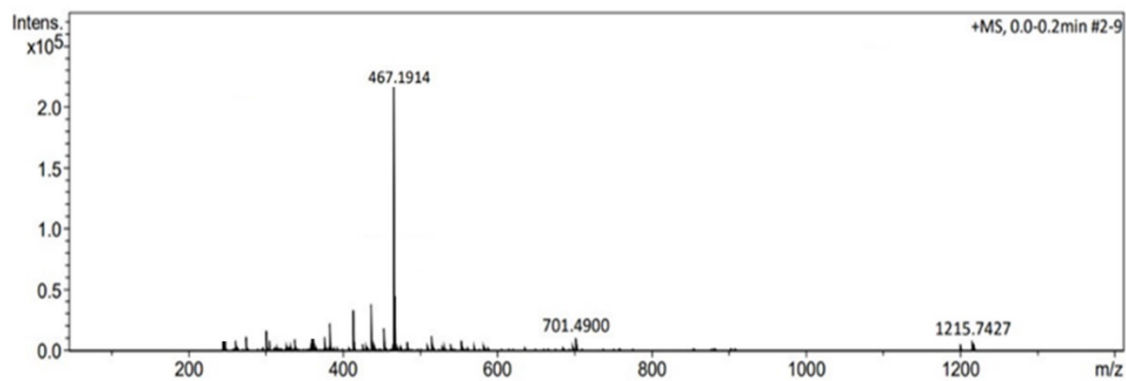
**Fig S3**: HRMS of CNPs showing one predominant molecular mass at m/z = 467

Fig S4: A) ^{1}H-NMR of CNPs B) ^{13}C -NMR of CNPs C) ^{13}C -DEPT-NMR of CNPs

Computational Details:

The molecular structure was designed using GAUSSIAN VIEW 6.0, and all computational studies were performed with the GAUSSIAN 09W program, the calculations were carried out using the density functional theory (DFT) method implemented in the series of programs within the computational package. For this computational study, we employed the B3LYP DFT functionals. The geometry optimization of the ground state was calculated step wise using the basis sets, 6–31 ++ G(d,p). The energy calculation of the first six vertical excited states was carried out using TD-DFT/IEFPCM 1model, with basis sets 6–31 ++ G(d,p), in a water solvent, we calculated the absorption spectra, circular dichroism spectra, and fluorescence spectra as well.
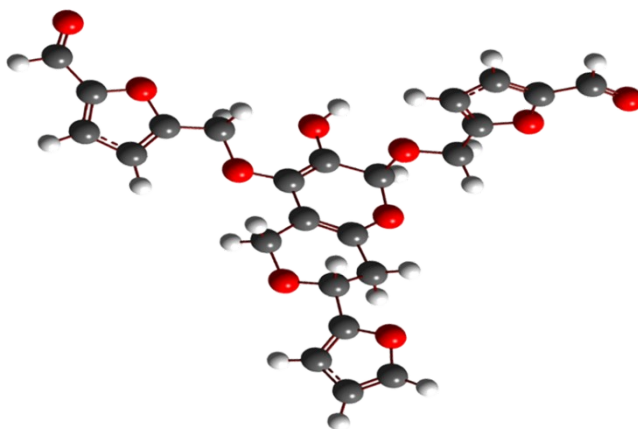
Fig S5: Optimized structure of the molecular fluorophore (F-467) obtained after DFT calculation
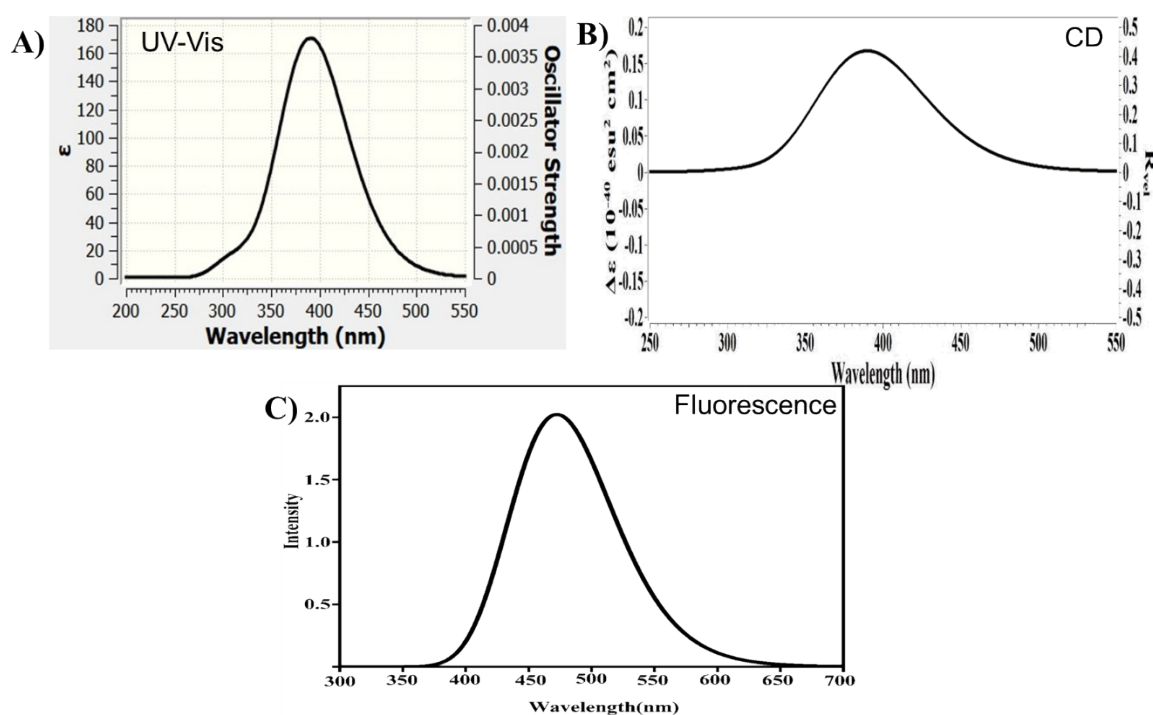
Fig S6: A) UV-Vis spectrum B) Circular dichroism spectrum C) Fluorescence of predicted molecular fluorophore (F-467) spectrum obtained after DFT and TD-DFT studies

Quantum yeild calculation:

The quantum yield of NSCNPs was determined with respect to quinine sulphate (Sigma-Aldrich, Germany, 99%) dissolving 0.1 M H2SO4 (quantum yield 54%) as standard [39]. The absorbances of various CNPs solutions and quinine sulphate solutions were measured in UV-Visible spectrophotometer (SHIMADZU UV-2450, Japan). The quantum yield of NSCNPs was calculated by using the following equation:

$$\frac{\emptyset}{\emptyset_{std}} = \frac{A_{std}}{A} \times \frac{I}{I_{std}} \times \frac{n^2}{n_{std}^2}$$

Where $\emptyset$ stands for quantum yield, "I" stands for measured integrated fluorescence intensity, n is the refractive index and A is the absorbance. "Std" refers to the standard fluorophore (quinine sulphate). The absorbance of all the solutions was kept less than 0.1 to avoid inner filter effects.

To find out the QY we have plotted integrated fluorescence intensities versus absorbance of various NSCNPs and standard solutions and the following equation was used:

$$\emptyset = \emptyset_{std} \times \frac{slope}{slope_{std}} \times \frac{n^2}{n_{std}^2}$$

where "Slope" represents the slope of the plot of absorbance versus integrated intensity[1].
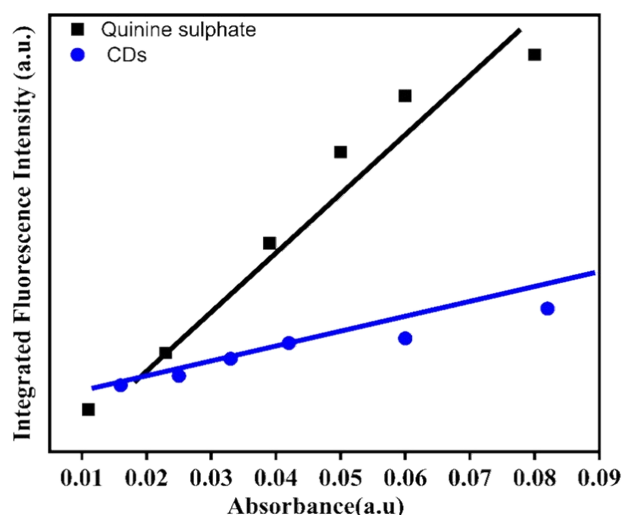
Fig S7: Quantum yield calculation of CNPs with respect to standard quinine sulphate
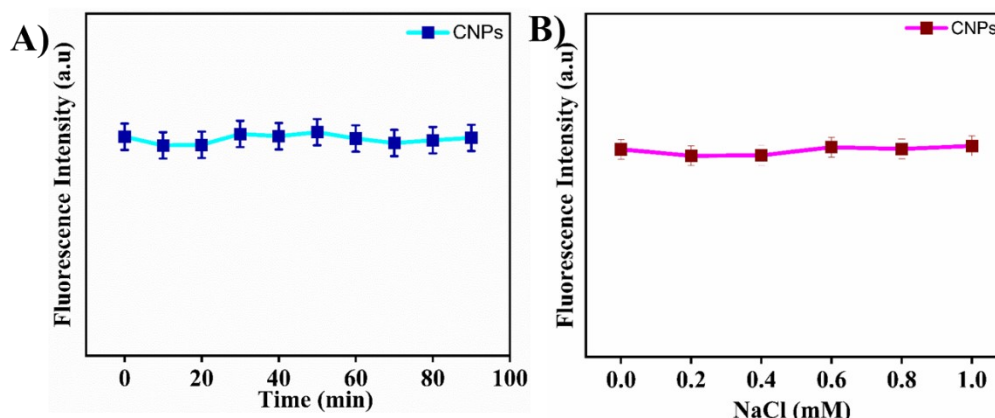
Fig S8: The effects of (A) UV-light illumination and (B) Ionic strength on the fluorescence emission of CNPs
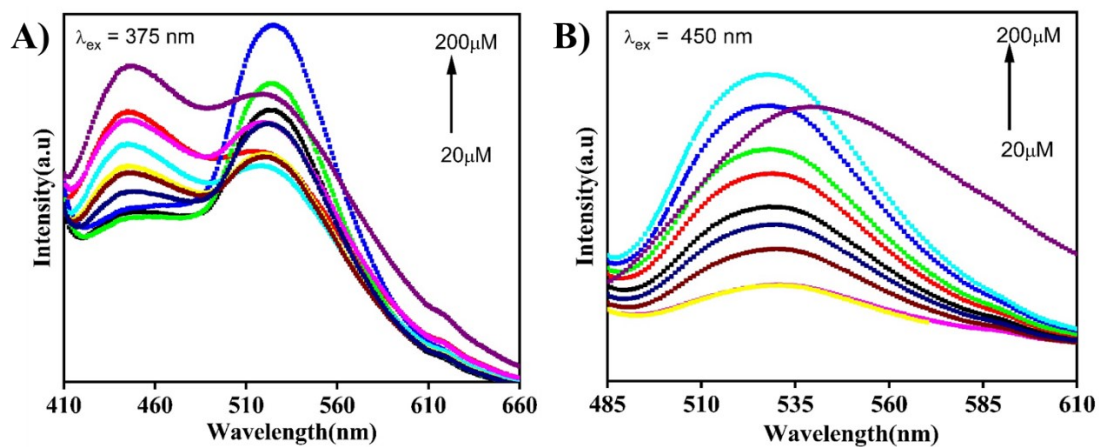
Fig S9: Ratiometric phenomena of CNPs in presence of UO_2^{2+} at A) 375 nm B) 450 nm excitation wavelength

Fig S10: Benesi–Hildebrand plot for the calculation of binding constant between CNPs and UO_2^{2+}

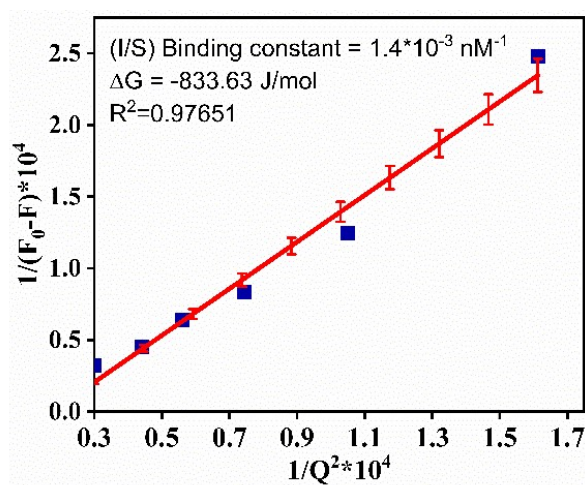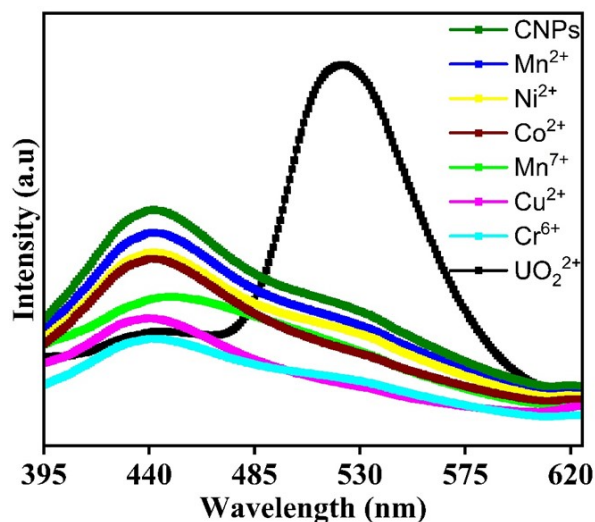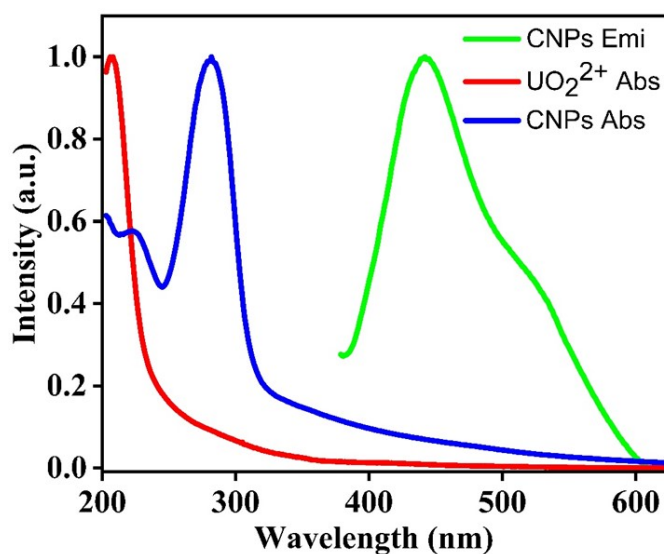**Fig S11**: Spectra of selective UO_2^{2+} sensing in presence of other metal ions

Fig S12: Absence of spectral overlap between emission of CNPs with absorption of UO_2^{2+}

Instrumentation of TAS:

The ultrafast transient absorption experiment setup utilizing a regenerative amplified Ti: sapphire laser system from Coherent (808 nm, 80 fs, 3 mJ/pulse, and 1 kHz repetition rate). The 30/70 beam splitter splits the 808 nm laser beam into two parts; the reflected part is used as pump beam for TOPAS Optical parametric Amplifier. It generates the pump beam for the TAS experiment within 290-1300 nm band. The transmitted part of 808 nm laser pulse again splits into two beams, one part with less than 10% is first transmitted through retro reflector stage to generate time delay between pump and probe followed by a neutral density filter and focused into CaF_2 crystal to generate a white light continuum (WLC) from 350 nm to 950 nm

used as probe beam. It is then focused on the sample by curved mirror. The transmitted/ reflected probe

Table S1: Comparison of LOD value for the sensing of UO_2^{2+}

Materials	Method	Linear range	LOD	Ref
T-PADAP	Colorimetry	$0–1.0 \times 10^{-5}$ (non-linear) (mol L^{-1})	4×10^3 (nmol L^{-1})	[2]
VPA-AuNPs	Colorimetry	0.5-10 µM	2µM (eyes), 1.07 µM (UV-Vis)	[3]

from the sample is then focused and collected by fiber coupled spectrometer. The synchronized optical chopper is used to chop the pump at the frequency of 500 Hz. The induced absorption change (ΔA) is calculated by difference in absorption of two adjacent probe.
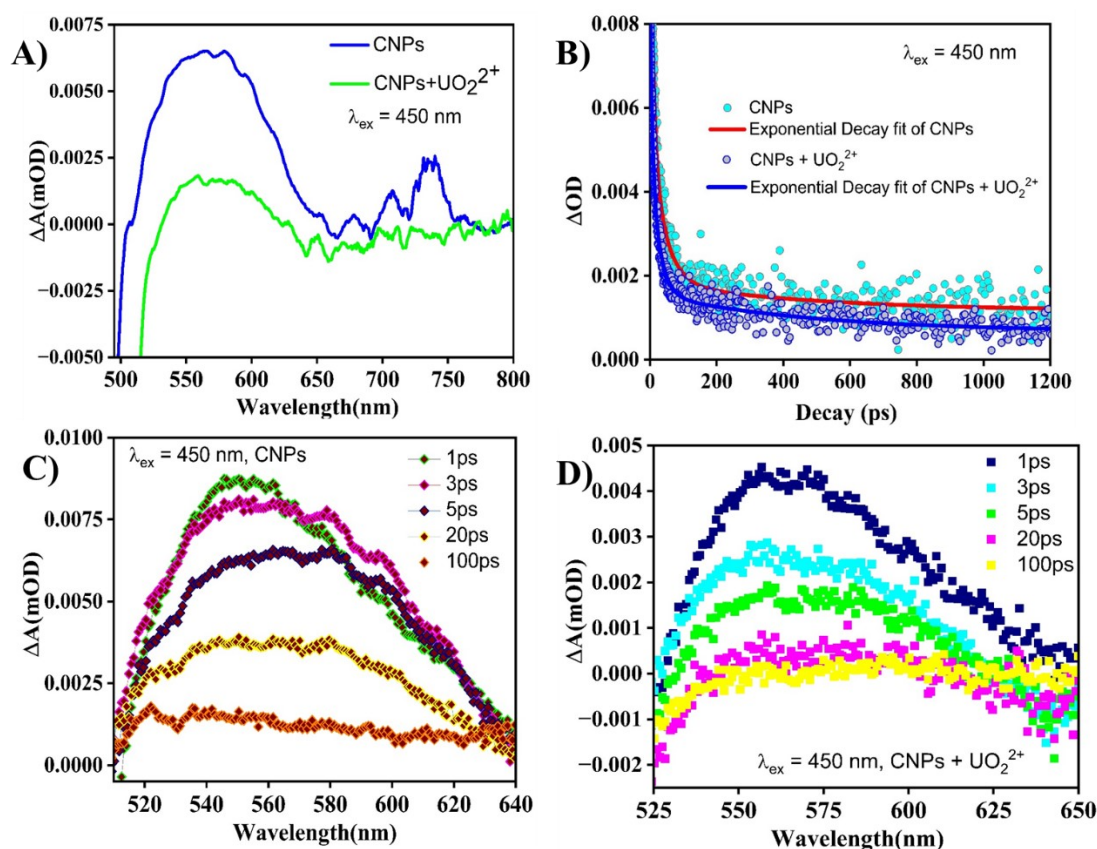
Fig S13: A) Transient absorption spectra of blue and green colour represent for CNPs and in presence of UO_2^{2+} at 450 nm; B) Decay curve of CNPs and in presence of UO_2^{2+} at 450 nm pump source; C) Time evolution of TA spectra of CNPs at 450 nm pump source; D) Time evolution of TA spectra of CNPs in presence of UO_2^{2+} at 450 nm pump source.

Rifampicin and Br-PADAP	Colorimetry	4-50 μM (rifampicin) 0.9-7 μM (Br-PADAP)	3.17 μM (rifampicin), 0.89 μM (Br-PADAP)	[4]
Fe3O4-Au@CdTe nanostructures	SERS-Fluorescence	0-320 nM	1.2 nM	[5]
DNAzyme-based hydrogels on Ag NP-grafted PAN nanorods	SERS	1 pM-0.1 μM	0.838 pM	[6]
AuNPs	Electrochemistry	2.4-48 μg L^{-1} 48-480 μg L^{-1}	0.3 μg L^{-1} 1 μg L^{-1}	[7]
Au-NP@CNTs/cat-1	Electrochemistry	0.49-170 μg L^{-1}	0.49 ± 0.01 μg L^{-1}	[8]
Dansyl modified peptide	Fluorescence	0-8 μM	83.2 nM	[9]
IR-DTB	Fluorescence	0-10 μM	93 nM	[10]
S-LH	UV-Vis	$0\text{-}10 \times 10^{-6}$ mol L^{-1}	1.46×10^{-8} Mol L^{-1}	[11]
AuNCs	UV-Vis	12-160 μM	1.86 μM	[12]
CNPs-Rho	Fluorescence	1.0 -100.0 μM	53 nM	[13]
CNPs-CdTe	Ratiometric Fluorescence	1 - 150 μM	0.07 μg/L	[14]
b-CNPs-r-CNPs	Fluorescence	0 μmol/L- 30.0 μmol	8.15 μmol/L	[15]
CQDs/MnFe$_2$O$_4$	Adsorption			[16]
CQDs@PAFP	Adsorption			[17]
CNPs	Fluorescence	0 to 75 ppm	0.71 ppm	[18]
N-CNPs/Hydrogel	Fluorescence		1.94 ppb/ 8.4 nM	[19]
Thenoyltrifluoroacetone (TTA)–Carbon Dot/Aerogel	Fluorescence			[20]
IFE between AuNPs - AuNCs	Ratiometric Fluorescence		0.84nM	[22]
CNPs (This work)	**Fluorescence**	**25–200 μM**	**12 nM**	

References:

[1] M. K. Mahto *et al.*, "Blue-Emissive Nitrogen-Doped Carbon Dots for Picric Acid Detection: Molecular Fluorescence Quenching Mechanism," *ACS Appl. Nano Mater.*, vol. 6, no. 9, pp. 8059–8070, May 2023, doi: 10.1021/acsanm.3c01523.

[2] J. Wen, S. Li, Z. Huang, W. Li, and X. Wang, "Colorimetric detection of Cu2+ and UO22+ by mixed solvent effect," *Dye. Pigment.*, vol. 152, pp. 67–74, 2018, doi: https://doi.org/10.1016/j.dyepig.2018.01.038.

[3] L. Zhang, D. Huang, P. Zhao, G. Yue, L. Yang, and W. Dan, "Colorimetric detection for uranyl ions in water using vinylphosphonic acid functionalized gold nanoparticles based on smartphone," *Spectrochim. Acta Part A Mol. Biomol. Spectrosc.*, vol. 269, p. 120748, 2022, doi: https://doi.org/10.1016/j.saa.2021.120748.

[4] Y. Lei *et al.*, "Smartphone-assisted colorimetric determination of uranyl ions in aqueous solutions," *New J. Chem.*, vol. 47, no. 10, pp. 4667–4673, 2023, doi: 10.1039/D2NJ05844H.

[5] C. Sun *et al.*, "Dual-mode fluorescence–SERS sensor for sensitive and selective detection of uranyl ions based on satellite Fe3O4-Au@CdTe nanostructure," *Sensors Actuators B Chem.*, vol. 325, p. 128644, 2020, doi: https://doi.org/10.1016/j.snb.2020.128644.

[6] X. He, X. Zhou, W. Liu, Y. Liu, and X. Wang, "Flexible DNA Hydrogel SERS Active Biofilms for Conformal Ultrasensitive Detection of Uranyl Ions from Aquatic Products," *Langmuir*, vol. 36, no. 11, pp. 2930–2936, Mar. 2020, doi: 10.1021/acs.langmuir.9b03845.

[7] S. Shi *et al.*, "Gold nanoparticles based electrochemical sensor for sensitive detection of uranyl in natural water," *J. Electroanal. Chem.*, vol. 880, p. 114884, 2021, doi: https://doi.org/10.1016/j.jelechem.2020.114884.

[8] J. Muñoz *et al.*, "Carbon nanotube-based nanocomposite sensor tuned with a catechol as novel electrochemical recognition platform of uranyl ion in aqueous samples," *Sensors Actuators B Chem.*, vol. 273, pp. 1807–1815, 2018, doi: https://doi.org/10.1016/j.snb.2018.07.093.

[9] L. Zhang *et al.*, "A novel fluorescence sensor for uranyl ion detection based on a dansyl-modified peptide," *Spectrochim. Acta Part A Mol. Biomol. Spectrosc.*, vol. 292, p. 122403, 2023, doi: https://doi.org/10.1016/j.saa.2023.122403.

[10] Y. Zhang *et al.*, "Near-infrared fluorescent probe based on cyanine scaffold for sensitive detection of uranyl ions in living cells and water samples," *Microchem. J.*, vol. 180, p. 107619, 2022, doi: https://doi.org/10.1016/j.microc.2022.107619.

[11] X. Wu *et al.*, "Designing a colorimetric sensor containing nitrogen and oxygen atoms for uranyl ions identification: Chromatic mechanism, binding feature and on-site application," *Sensors Actuators B Chem.*, vol. 307, p. 127681, 2020, doi: https://doi.org/10.1016/j.snb.2020.127681.

[12] D. Zhang, Z. Chen, H. Omar, L. Deng, and N. M. Khashab, "Colorimetric Peroxidase Mimetic Assay for Uranyl Detection in Sea Water," *ACS Appl. Mater. Interfaces*, vol. 7, no. 8, pp. 4589–4594, Mar. 2015, doi: 10.1021/am507361x.

[13] D. Wang *et al.*, "Aggregation enhanced FRET: A simple but efficient strategy for the ratiometric detection of uranyl ion," *J. Hazard. Mater.*, vol. 454, p. 131497, 2023, doi: https://doi.org/10.1016/j.jhazmat.2023.131497.

[14] X. Chen *et al.*, "Rapid and On-Site Detection of Uranyl Ions via Ratiometric Fluorescence Signals Based on a Smartphone Platform," *ACS Appl. Mater. Interfaces*, vol. 10, no. 49, pp. 42225–42232, Dec. 2018, doi: 10.1021/acsami.8b13765.

[15] J. Qian *et al.*, "Field-portable ratiometric fluorescence imaging of dual-color label-free carbon dots for uranyl ions detection with cellphone-based optical platform," *Chinese Chem. Lett.*, vol. 31, no. 11, pp. 2925–2928, 2020, doi: https://doi.org/10.1016/j.cclet.2020.05.004.

[16] S. Huang *et al.*, "Dual functional nanocomposites of magnetic MnFe2O4 and fluorescent carbon dots for efficient U(VI) removal," *Chem. Eng. J.*, vol. 368, pp. 941–950, 2019, doi: https://doi.org/10.1016/j.cej.2019.03.015.

[17] M. E. Mahmoud, N. A. Fekry, and A. M. Abdelfattah, "Removal of uranium (VI) from water by the action of microwave-rapid green synthesized carbon quantum dots from starch-water system and supported onto polymeric matrix," *J. Hazard. Mater.*, vol. 397, p. 122770, 2020, doi: https://doi.org/10.1016/j.jhazmat.2020.122770.

[18] Z. Wang, Y. Lu, H. Yuan, Z. Ren, C. Xu, and J. Chen, "Microplasma-assisted rapid synthesis of luminescent nitrogen-doped carbon dots and their application in pH sensing and uranium detection," *Nanoscale*, vol. 7, no. 48, pp. 20743–20748, 2015, doi: 10.1039/C5NR05804J.

[19] Q. Wang, T. Han, C. Miao, W. Qin, and X. Wu, "A fluorescent N-doped carbon dot-hydrogel composite for concurrent selective detection and local hot spot promoted adsorption of uranium(vi)," *Environ. Sci. Water Res. Technol.*, p., 2023, doi: 10.1039/D3EW00527E.

[20] S. Dolai, S. K. Bhunia, L. Zeiri, O. Paz-Tal, and R. Jelinek, "Thenoyltrifluoroacetone (TTA)–Carbon Dot/Aerogel Fluorescent Sensor for Lanthanide and Actinide Ions," *ACS Omega*, vol. 2, no. 12, pp. 9288–9295, Dec. 2017, doi: 10.1021/acsomega.7b01883.

[21] H.-R. Nan *et al.*, "An inner-filter-effect based ratiometric fluorescent sensor for the detection of uranyl ions in real samples," *Anal. Methods*, vol. 14, no. 5, pp. 532–540, 2022, doi: 10.1039/D1AY02017J.